Fundamental Research 4 (2024) 123–130

Contents lists available at ScienceDirect

Fundamental Research

journal homepage: http://www.keaipublishing.com/en/journals/fundamental-research/

Article

# Femtosecond laser 3D printed micro objective lens for ultrathin fiber endoscope

Bozhe Li [a,b], Changrui Liao [a,b,*], Zhihao Cai [a,b], Jie Zhou [a,b], Cong Zhao [a,b], Liqing Jing [a,b], Jiaqi Wang [a,b], Cong Xiong [a,b], Lei Xu [c], Ying Wang [a,b], Yiping Wang [a,b]

[a] Key Laboratory of Optoelectronic Devices and Systems of Ministry of Education/Guangdong Province, College of Physics and Optoelectronic Engineering, Shenzhen University, Shenzhen 518060, China

[b] Shenzhen Key Laboratory of Photonic Devices and Sensing Systems for Internet of Things, Guangdong and Hong Kong Joint Research Centre for Optical Fibre Sensors, Shenzhen University, Shenzhen 518060, China

[c] School of Electronic and Communication Engineering, Shenzhen Polytechnic University, Shenzhen 518055, China

ARTICLE INFO

*Article history:*
Received 1 February 2022
Received in revised form 26 May 2022
Accepted 29 May 2022
Available online 19 June 2022

*Keywords:*
Femtosecond laser
Two-photon polymerization
3D printing
Micro objective lens
Fiber endoscope

ABSTRACT

The most important optical component in an optical fiber endoscope is its objective lens. To achieve a high imaging performance level, the development of an ultra-compact objective lens is thus the key to an ultra-thin optical fiber endoscope. In this work, we use femtosecond laser 3D printing to develop a series of micro objective lenses with different optical designs. The imaging resolution and field-of-view performances of these printed micro objective lenses are investigated via both simulations and experiments. For the first time, multiple micro objective lenses with different fields of view are printed on the end face of a single imaging optical fiber, thus realizing the perfect integration of an optical fiber and objective lenses. This work demonstrates the considerable potential of femtosecond laser 3D printing in the fabrication of micro-optical systems and provides a reliable solution for the development of an ultrathin fiber endoscope.

## 1. Introduction

The endoscope is a common image-based inspection instrument. An endoscope can enter a narrow channel to observe the internal status of a specific structure under test. In the medical field, doctors can observe the morphological and pathological changes in human body cavities and internal organs using an endoscope [1,2], and the endoscope has been used widely in clinical scenarios such as examinations [3] and minimally invasive surgery [4]. In the industrial field, endoscopes have been widely used in pipeline detection [5], aerospace [6], artificial intelligence [7], and other applications. As a result of rapid developments in micro/nano machining technology, the size of a typical endoscope has been reduced greatly, but current endoscopes still cannot fully meet the endoscopic imaging requirements for certain ultra-thin pipes used in medical and industrial applications. Researchers have been developing innovative methods of how to reduce the size of the endoscopes while maintaining the required imaging quality in different applications [8,9]. Several micromachining technologies are commonly used in the micro-optics field, including diamond turning [10], ultra-precision milling [11], ultra-precision polishing [12], magnetorheological polishing [13], and ion beam polishing [14]. Although these technologies have sufficient high machining precision, they cannot be used to fabricate micro multi-lens systems. Therefore, the development of a new method for micro-optics micromachining and precision assembly has major research value.

Femtosecond laser-induced two-photon polymerization (TPP) is an optical additive micromachining method that has achieved the highest reported accuracy to date [15], and TPP has been used widely in micro/nanophotonics [16], microelectromechanical systems (MEMS) [17], and microfluidics [18]. Since the probability of occurrence of TPP is directly proportional to the square of the photon density [19], this nonlinear threshold effect can limit the polymerization effect to a tiny region, and can even break the Abbe diffraction limit. The printed feature size can thus reach 100 nm or less [20–23]. At present, many research groups are working on the TPP printing of micro-optical systems, including microlens arrays [24], optical phase plates [25–27], fiber gratings [28–30], fiber couplers [31,32], and fiber interferometers [33–36]. More interestingly, TPP can be used to fabricate complex freeform optics with high quality [32,37,38], and can even be used to add air gaps accurately to enable the fabrication of microlens groups [39–41]. Dietrich et al. devel-

* Corresponding author.
*E-mail address:* cliao@szu.edu.cn (C. Liao).

https://doi.org/10.1016/j.fmre.2022.05.026

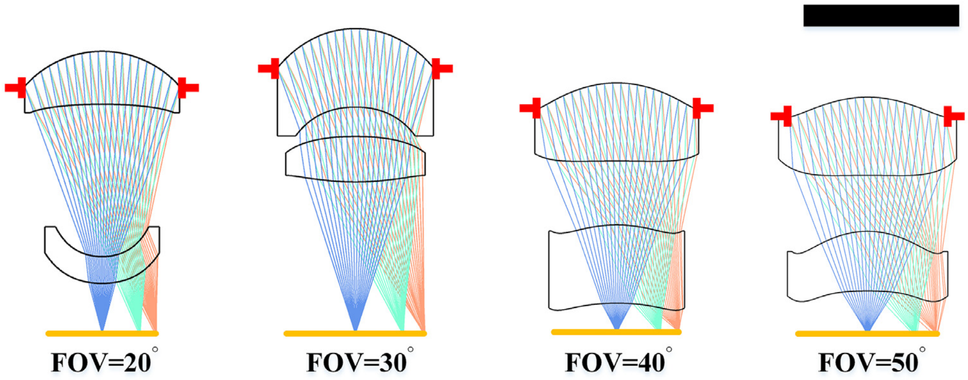


**Fig. 1. Optical designs of micro objective lenses after optimization in Zemax.** The red marks indicate the entrance pupil of these four micro objective lenses. The yellow lines indicate the position of image plane. (scale bar: 100 $\mu$m). (For interpretation of the references to color in this figure legend, the reader is referred to the web version of this article.)

**Table 1**
**Parameters of the micro objective lenses.**

| FOV | F-number | Focal length | Image plane diameter |
|---|---|---|---|
| 20° | 2 | 200 $\mu$m | 69.7 $\mu$m |
| 30° | 1.67 | 167 $\mu$m | 90.2 $\mu$m |
| 40° | 1.1 | 110 $\mu$m | 80.5 $\mu$m |
| 50° | 0.95 | 95 $\mu$m | 90.0 $\mu$m |

oped a series of beam shaping elements composed of multiple lenses and achieved extremely high coupling efficiency [40]. Thiele et al. [41] used TPP to print microlens groups on a CMOS chip and realized the visual effect of the fovea. When compared with traditional lens fabrication methods, TPP offers great micromachining flexibility and can realize direct integration of multiple microlenses to resolve assembly problems. In this work, we use TPP to print a series of micro objective lenses and investigate the morphology and imaging performances of these lenses, which are highly consistent with the simulation results. Ultimately, four micro objective lenses with different fields of view (FOVs) are printed and integrated on the end face of a single imaging fiber for the first time to achieve simultaneous endoscopic imaging. This work thus provides a reliable solution for the development of ultrathin optical fiber endoscopes.

## 2. Lens design and fabrication

### 2.1. Optical design

The Sequential mode of Zemax commercial optical design software was used to simulate and optimize the micro objective lenses for endoscopy applications in this work. The optical design diagram of micro objective lenses is shown in Fig. 1, where the blue, green, and orange lines represent the ray tracing in the different FOVs. The four objective lenses all use a doublet lens structure. The entrance pupil of the lens group is designed to occur at the first lens, and thus limits the angle of the imaging beam. This approach ensures that all light that passes through the second lens is received by the first lens, minimizing the impact of any light that passes directly through the second lens and onto the final image. The diameter of the entrance pupil for the four objective lenses is set at 100 $\mu$m, and the image plane is in the form of a circle with a diameter of less than 100 $\mu$m. Detailed parameters for the four objective lenses are listed in Table 1. Considering the dimensional error that may occur during fabrication, a margin of 2% is added to each edge of each lens, but this adjustment will result to a slight increase of less than 2 um in the size of the entrance pupil.

In terms of aberration control, narrow-band light illumination within the wavelength range of 550 ± 10 nm is used to reduce the effects of chromatic aberration. In addition to chromatic aberration, the objective lens is required to correct all monochromatic aberrations, including defocusing, spherical aberrations, coma, astigmatism, field curvature, and distortion. Because the fabrication method imposes no restrictions on the surface shape of the lens, the surface of the objective lens is set to be a high-order and even-order asphere, which can be expressed as shown in Eq. 1:

$$Z(r) = \alpha_0 + \frac{cr^2}{1 + \sqrt{1 - (1 + k)c^2 r^2}} + \sum_{i=1}^{10} \alpha_i r^{2i} \quad (1)$$

Here, $Z(r)$ is the sag, which is the $z$-component of the surface displacement from the vertex; $r$ is the radial ray coordinate in lens units; $c$ is the fundamental curvature at the vertex; $k$ is the conic constant; $\alpha_i$ describes the surface deviation from the axially symmetric quadric surface specified by $c$ and $k$. $\alpha_i$ and $k$ provide additional degrees of freedom to compensate for the aberrations when compared with the spherical surface typically used in conventional lens design. A 10-order even aspherical surface is used in this work.

After optimization, the ultimate designs can effectively eliminate most monochromatic aberrations. Among all the monochromatic aberrations, field curvature and distortion are two important aberrations that should be taken into consideration in the design of micro objective lenses, but both aberrations have a strong dependence on the FOV. The field curvature is proportional to the square of the FOV, and the distortion is proportional to the third power of the FOV. Therefore, for an optical system with a large FOV, these two aberrations are very difficult to correct. However, through the aspheric lens design, the distortion is well controlled to within 3% and the field curvature is controlled to within 5 $\mu$m here (Fig. S1). The spot diagrams in Fig. S1 indicated the diffraction-limited performance (with a Strehl ratio of > 0.8) of most micro objective lenses with different FOVs.

### 2.2. Lens fabrication

Based on the lens data exported from the optical design, a 3D model of the objective lens was drawn using computer-aided design (CAD) software, and it was noted that a development channel should be reserved in the lens model. The designed 3D model was then first printed on a glass slide coated with indium tin oxide (ITO) via TPP. The TPP 3D printing system developed by our laboratory, used a layer-by-layer scanning strategy (Fig. S2). The slicing layer spacing and the line spacing were set to 0.2 $\mu$m and 0.3 $\mu$m, respectively. The femtosecond laser used in this step had a central wavelength of 780 nm, a pulse width of 100 fs, and a repetition rate of 80 MHz. The femtosecond laser pulses were focused using a 25 × oil immersion objective with a numerical aperture (NA) of 0.8. The fabrication resolution of the TPP 3D printing system in X, Y, and Z directions can reach 100 nm, 100 nm, and 300 nm, respectively

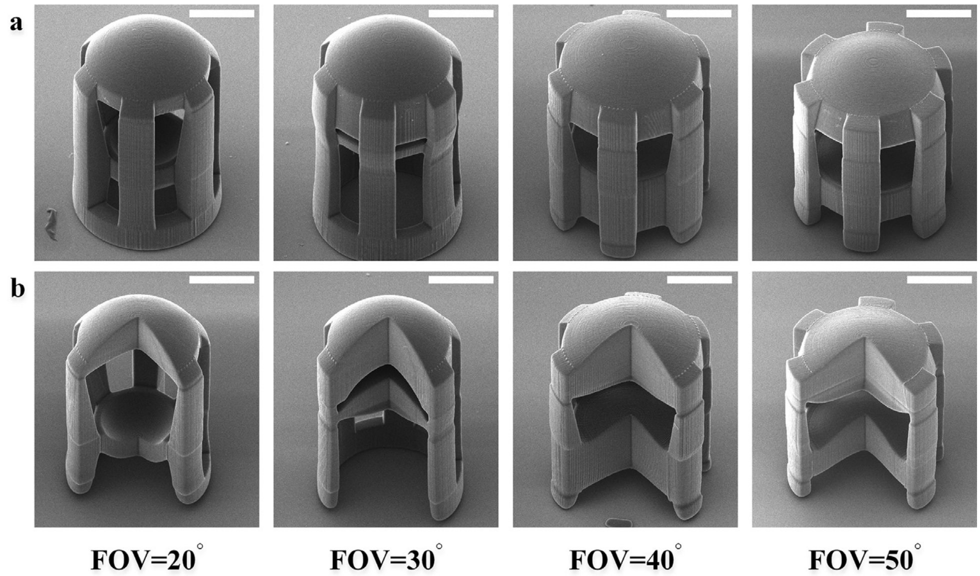


**Fig. 2. Scanning electron microscope (SEM) images of the 3D printed micro objective lenses.** (a) Overall views of the 3D printed micro objective lenses. From left to right, the images show the micro objective lenses with FOVs of 20°, 30°, 40°, and 50° (scale bars: 50 $\mu$m). (b) Corresponding 90° section views of the printed objective lenses shown in part (a) (scale bars: 50 $\mu$m). (For interpretation of the references to color in this figure legend, the reader is referred to the web version of this article.)

[30]. The processing precision of TPP is strongly related to laser pulse energy and scanning speed. Under the optimization of laser pulse energy (0.2 nJ) and scanning speed (50 mm/s), an ideal manufacturing result is obtained. (Fig. S3). Material dispersion is another important parameter in the design of high-quality optical systems. Since our endoscope objective lens was printed with a single type of photoresist, chromatic aberrations such as the longitudinal and transverse chromatic aberrations cannot be corrected effectively. To reduce the effects of these chromatic aberrations as far as possible, the IP-S photoresist (Nanoscribe GmbH, Germany) ($n_{588nm}$ = 1.5067, $\nu$ = 46.16) [42] with low dispersion was selected for the TPP printing step. The printing time for each designed endoscope objective was approximately 15 min. After printing, the sample was immersed in propylene glycol methyl ether acetate (PGMEA) for 15 min to remove any uncured photoresist and was then soaked in isopropanol for 3 min to remove the remaining PGMEA. Finally, the sample was extracted from the isopropanol and the designed endoscope objective was obtained after the isopropanol had been volatilized completely.

## 3. Results and discussion

Scanning electron microscope (SEM) images of the fabricated micro objective lenses with FOVs of 20°, 30°, 40°, and 50° are shown in Fig. 2. Each micro objective lens has an equally spaced support structure to ensure that air separation is maintained between the lenses. These support structures are approximately 20 $\mu$m thick. As shown in Fig. 2, each micro objective lens has a relatively smooth surface, but some micromorphological features that resulted from the layer-by-layer printing process can still be observed. In particular, in the areas where the curvature changes sharply, e.g., the lens top, this morphology is more obvious. The presence of these features can be explained by the limited slicing layer spacing used in the printing process. To illustrate the internal structures of the micro objective lenses more clearly, Fig. 2b shows the corresponding 90° sections of each of the micro objective lenses. Both the surface shapes and the spacing of the air gaps are well presented.

To characterize the morphologies of the printed lenses quantitatively, a white-light interferometer (Atometrics, EX230) was used to measure the surface topography of each lens. The measurement result was then compared with the designed topography. Fig. 3a shows the designed 10-order even aspherical surface, where the curvature radius of the aspherical surface is 88.6 $\mu$m. Fig. 3b shows the topography of the printed lens measured by optical interferometry, where the curvature radius obtained by fitting is 87.2 $\mu$m. The root mean square (RMS) error between the designed and measured results is calculated to be 349 nm. This dimensional error is mainly caused by the layer-by-layer printing process, and by subsequent structural shrinkage or deformation during the development process. The fundamental factors causing these errors are the laser power used, the scanning speed, the surface tension of the photoresist, and the volatilization process. Therefore, the fabrication parameters listed above must be optimized repeatedly to improve the printing quality.

The imaging performances of the printed lenses were also investigated. The experimental setup is illustrated in Fig. 4a. The test chart was illuminated by a light-emitting diode (LED) plane light source from the rear. The printed micro objective lens was placed approximately 20 mm away from the test chart. The image of the test chart was then observed using a microscopic imaging system, which consisted of an objective with an NA of 0.42, a tube lens, a bandpass filter for the 550 ± 10 nm range, and a charge-coupled device (CCD) camera. Fig. 4b shows the two test charts used in the experiments. The top image shows a customized FOV test chart consisting of concentric rings drawn at an azimuthal angle separation for a 10°FOV. The other chart (bottom image) is the 1951 USAF resolution test chart (Thorlabs).

The principle for the FOV test can be expressed using Eq. 2:

$$\mathrm{FOV} = 2\arctan(r/l) \tag{2}$$

where $r$ is the radius of the FOV, and $l$ is the object distance of 20 mm used in the tests. The results of the FOV tests are shown in Fig. 5a, where two, three, four, and five concentric rings can be observed clearly from the four printed micro objective lenses corresponding to the FOVs of 20°, 30°, 40°, and 50°, respectively. Since the micro objective lens is printed in one piece, its support structure is composed of the same polymer material used to form the lens. As a result, the micro objective lens contains no light-blocking structures and has good light transmission performance. But this also means that the structure would be affected by stray light. To analyze the effects of stray light, the 3D printing model was imported into the Non-Sequential mode of the Zemax software to perform a simulated imaging analysis. The simulation results are shown in Fig. 5b, which are roughly consistent with the corresponding exper-

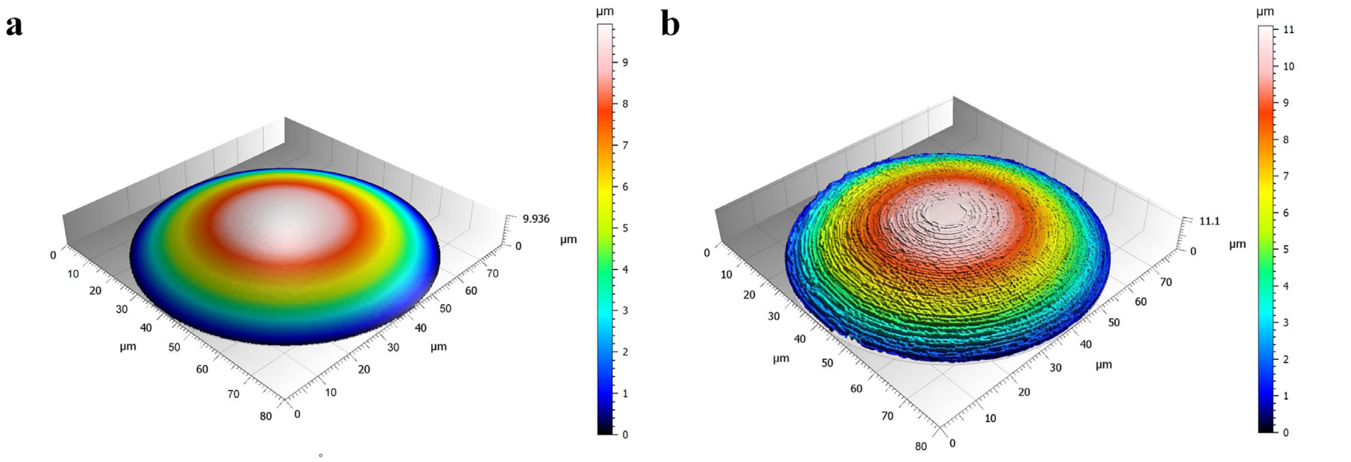


**Fig. 3. Lens surface topography test diagram.** (a) Surface topography of the designed lens. (b) Topography of the printed lens measured by optical interferometry.

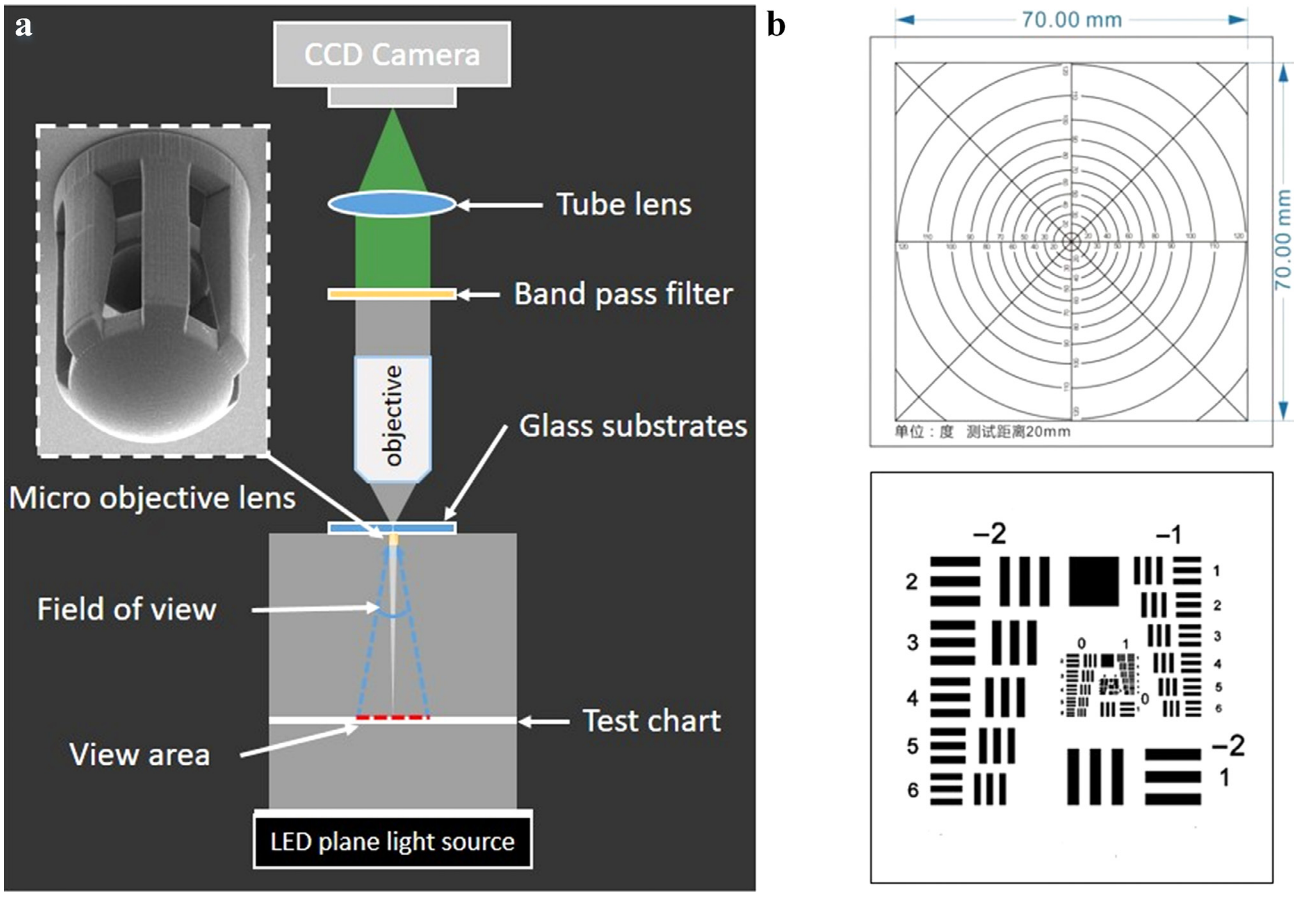


**Fig. 4. Micro objective lens imaging testing system.** (a) Schematic diagram of the imaging testing system. (b) Customized FOV test chart (top) and 1951 USAF resolution test chart (bottom).

imental results. The slight difference between simulations and real experiments resulted from the fact that the micro objective lenses are designed with infinite object distance, while the object distance is finite in real imaging. The above results verified that complex optical designs can be realized well by the TPP process.

Resolution is another important parameter for objective lenses. Fig. 6 shows the result of resolution tests performed using the 1951 USAF resolution chart. Although a narrow-band filter was used, this optical system still had a certain level of chromatic aberration, and thus the images have slightly blurred edges rather than sharp edges. Fig. 6a shows the image of the resolution chart acquired using an objective lens with a FOV of 20°. It could be seen that the limited resolution element was the element 2 in group 2, achieving a resolving power of 4.49 lp/mm, and this power corresponded to a line width of 111.36 $\mu$m and azimuth resolution of 19′8″ (The calculation method of line width and azimuth resolution is discussed in the Supplementary Information). Fig. 6b–d show the imaging results acquired using the objective lenses with FOVs of 30°, 40°, and 50°, where azimuth resolutions of 21′29″ (element 1 of group 2), 30′23″ (element 4 of group 1), and 34′6″ (element 3 of group 1) were achieved, respectively.

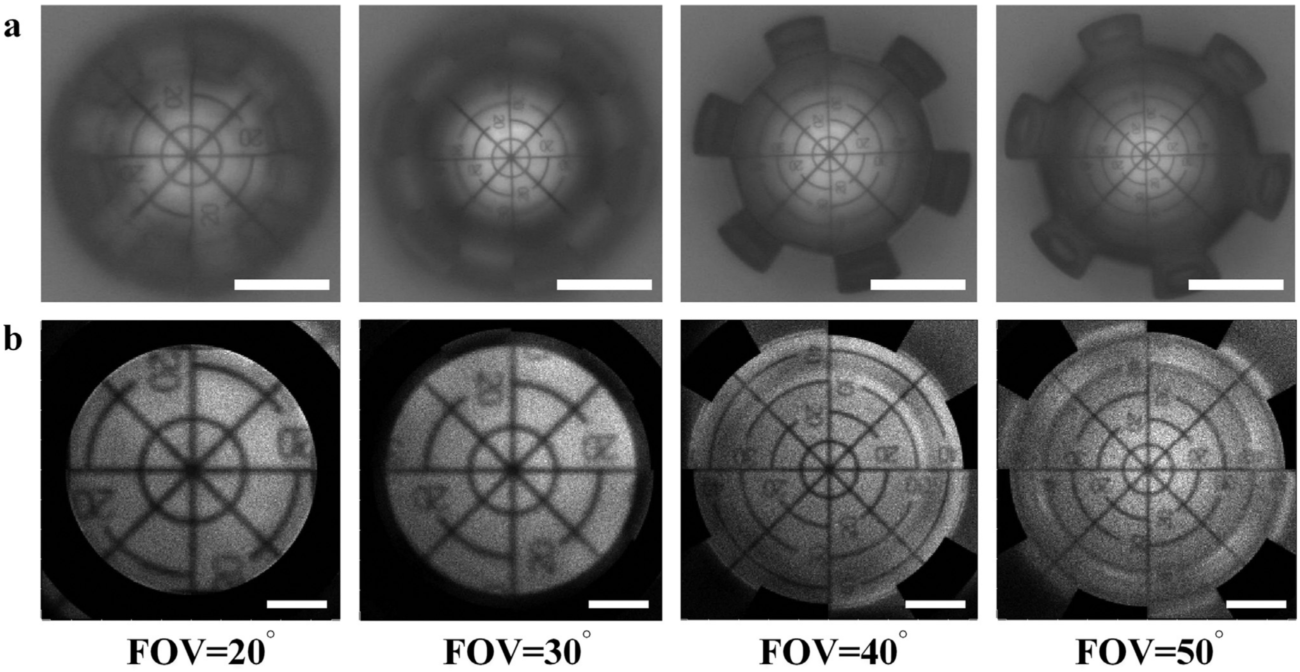


**Fig. 5. Measurement and simulation results for the FOVs of the micro objective lenses.** (a) Measured images of the micro objective lenses obtained using the FOV test chart (scale bars: 50 $\mu$m). (b) Simulated images of the micro objective lenses (scale bars: 20 $\mu$m).

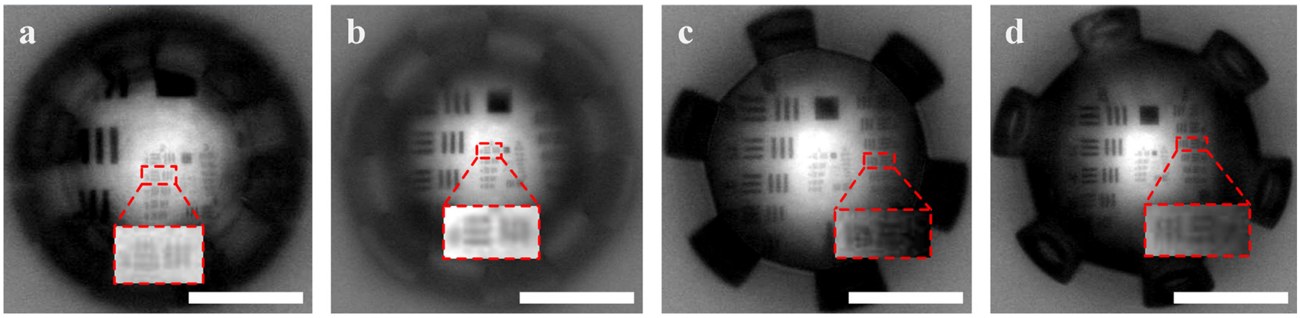


**Fig. 6. Resolution measurement results for the micro objective lenses.** The red line frames the limit resolution elements. (a) FOV = 20°. (b) FOV = 30°. (c) FOV = 40°. (d) FOV = 50° (scale bars: 50 $\mu$m). (For interpretation of the references to color in this figure legend, the reader is referred to the web version of this article.)

The modulation transfer function (MTF) provides a useful method to evaluate the performance of an optical system in terms of its ability to restore object details. Therefore, we simulated and tested the MTF curves of each printed objective lens. Fig. 7 shows the normalized MTF curves for the four micro objective lenses with different FOVs, where the solid lines represent the simulated MTF curves and the dotted lines represent the MTF curves acquired via knife-edge measurements. These curves show that there are some differences between the measured and simulated results. One possible reason for these differences is that the layer-by-layer printing method causes the lens surface to have a fine stepped shape rather than a perfectly spherical shape. In addition, the printed lens will shrink unevenly and uncontrollably during the development process. Although there are certain observable differences between the measurements and the simulations, these results still demonstrate the satisfactory imaging quality of the lenses. Modulation regimes of higher than 10% were demonstrated at frequencies of less than 450 lp/mm.

Finally, the micro objective lenses were printed onto the end face of an imaging fiber to realize the microendoscopic application of the lenses. The imaging fiber has an external diameter of 700 $\mu$m, an effective imaging area with a diameter of 460 $\mu$m, and 12,000 cores with the same diameter of 4 $\mu$m. The interval between adjacent cores is 1 $\mu$m. To match the fiber specifications, we redesigned the micro objective lenses, and the design diagram was shown in Fig. 8a. To distinguish between the imaging effects of the endoscope objectives with the different FOVs, we fixed the image plane size and the aperture size of the objective at 100 $\mu$m and 120 $\mu$m, respectively.

The experimental setup used to test the fiber endoscope is shown in Fig. 8b. At the output end of the imaging fiber, a microscope objective lens (50×, NA = 0.42) was used to enlarge the images from the fiber for input to a CCD camera. Fig. 8c shows the picture of printed objective lenses on the fiber end face. The four micro objective lenses formed a square array. The image plane diameter for each micro objective lens was approximately 100 $\mu$m, each covering approximately 700 pixels of the imaging fiber. Fig. 8d shows the imaging results obtained from the fiber endoscope under transmitted light illumination; images of the element 2 from group 0 in the resolution chart can be observed clearly, and larger areas can be seen through the lenses with larger FOVs, but the image resolution also decreases accordingly. Since most endoscopic imaging applications use reflected light illumination, we also investigated the imaging performance of the fiber endoscope under reflected

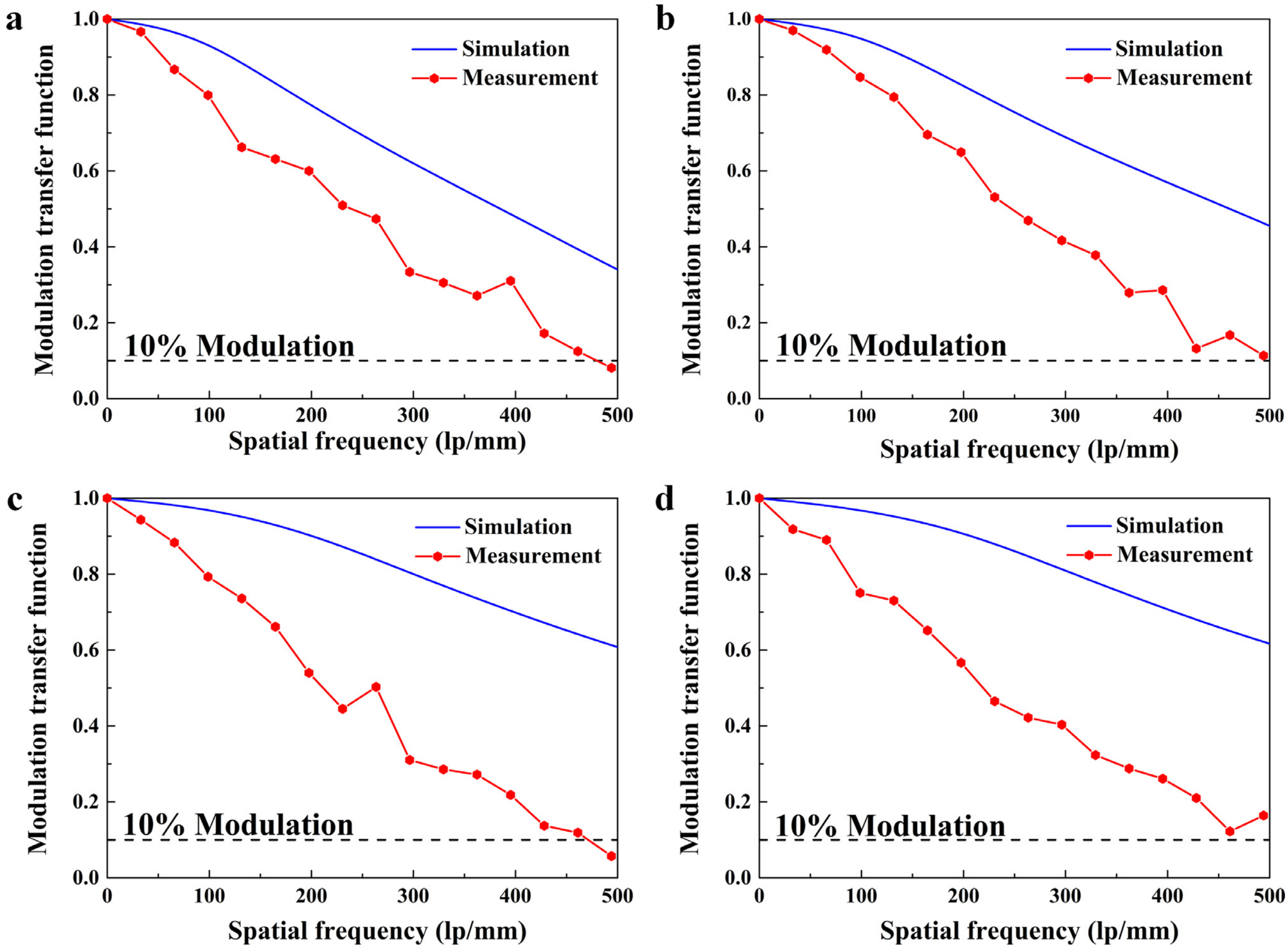


**Fig. 7. Simulated and measured MTFs of the four micro objective lenses.** (a) FOV = 20°. (b) FOV = 30°. (c) FOV = 40°. (d) FOV = 50°.

light illumination conditions (Fig. S4). Fig. 8e shows the results of imaging of adult fingers under reflected light illumination, in which the contours and postures of the fingers can be observed. All the above results have demonstrated that multiple objectives with different FOVs are well integrated on the end face of the imaging fiber. The objective lens with the largest FOV can be used to locate the observed object, and the other lenses with smaller FOVs can be used for fine imaging. However, the imaging quality of the fiber endoscope is not satisfying at this stage. There are two main factors affecting the imaging quality of fiber endoscopes. One factor is the resolution of the objectives which directly determines the image quality received by the fiber. The other factor is the intrinsic parameter of the imaging fiber such as the diameter and density of fiber cores. For optical fiber endoscopes, the image plane size of the objective lens on the end of the optical fiber should be designed as large as possible if there is sufficient space. In this way, a single objective could cover more fiber cores. Increasing the density of fiber cores on the imaging fiber is another approach, while the size of the imaging plane of the objective lens remains the same. As a result, the imaging quality of optical fiber endoscopes is enhanced owing to higher pixels of one image transmitted by the imaging fiber. Thus, in the ultrathin endoscopy imaging, in which the imaging fiber with an extremely small diameter is needed, we could choose an imaging fiber with high-density fiber cores. In applications where the diameter of the imaging fiber is not strictly required, larger imaging fibers can be selected because they contain more pixels.

In comparison, the imaging quality of commercial electronic endoscopes is much better than that of optical fiber endoscopes since the receiver of the electronic endoscope is a CMOS chip that has more pixels in a small image plane than the imaging fiber. Therefore, even though the objective lens printed by the TPP printing system can achieve high resolution, the resolution of ultimate imaging is relatively poor due to the limited number of fiber cores covered by a single objective lens. However, the ultrathin fiber endoscopes fabricated in our work, if being used in clinic, could identify lesions in narrow apertures or cracks, allowing doctors to examine or treat very small organs or body parts in a minimally invasive manner. In our further work, we would employ an imaging fiber with much denser fiber cores for fabricating fiber endoscopes to obtain better imaging quality.

## 4. Conclusion

In this work, we have successfully prepared a series of micro objective lenses with different FOVs for fiber endoscopic imaging applications by TPP. This nanoscale printing method can realize complex micro-optical systems perfectly, including aspheric structures. The micro objective lenses prepared by this method demonstrated acceptable imaging performances and thus offer a new approach for the realization of ultrathin fiber endoscopes. Next, we intend to conduct in-depth research into microlens design optimization and functional regulation

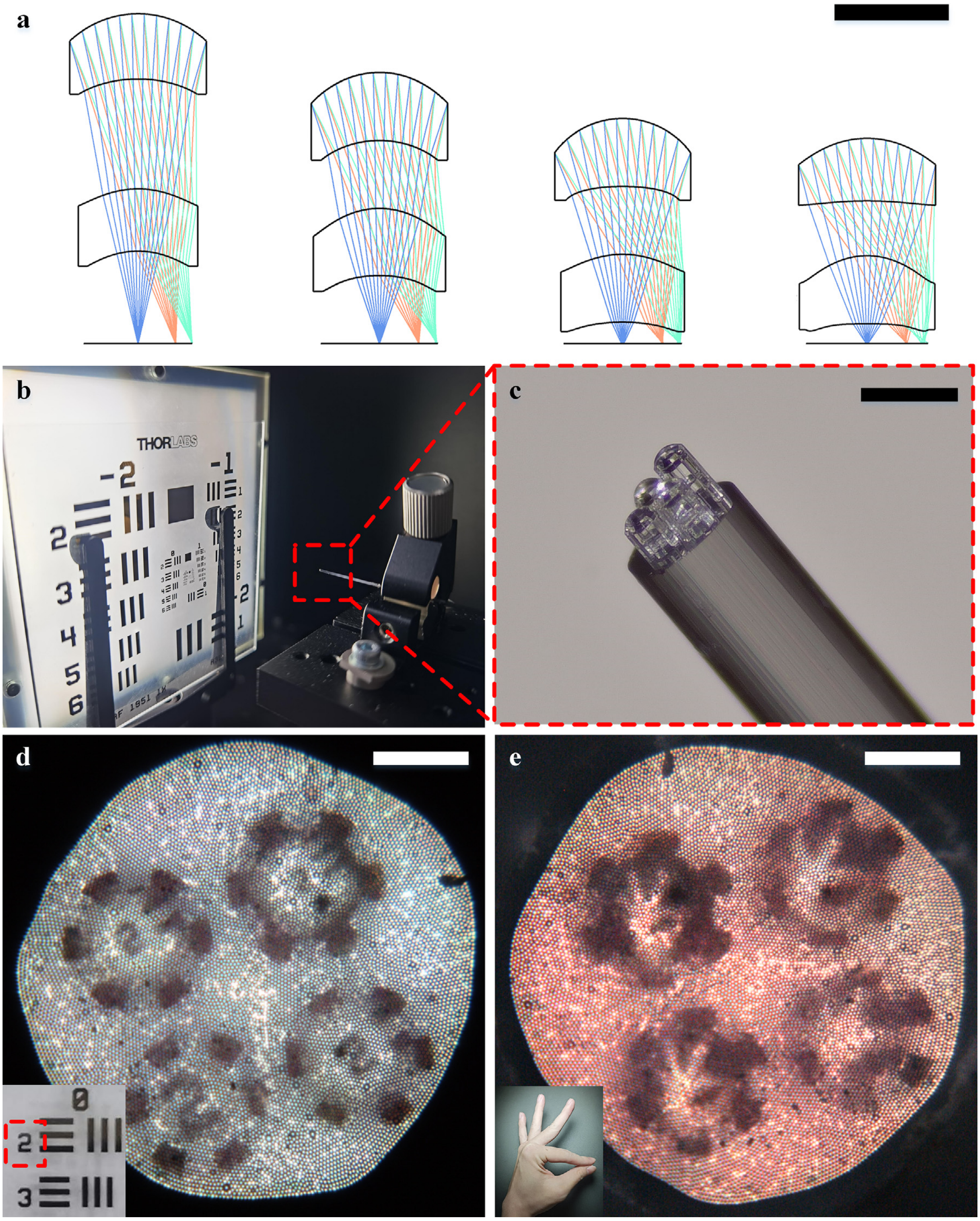


**Fig. 8. Four micro objective lenses printed directly on an imaging fiber.** (a) The optical design of micro objective lenses as optimized in Zemax (scale bar: 100 $\mu$m). (b) The imaging test system used for fiber endoscope. (c) Optical microscope image of the printed micro objective lenses on the fiber end (scale bar: 400 $\mu$m). (d) Resolution chart images acquired by fiber endoscope under transmitted light illumination. The diagram on the lower left shows the picture of the object observed (scale bar: 100 $\mu$m). (e) Adult finger images acquired by fiber endoscope under reflected light illumination. The diagram on the lower left shows the picture of the object observed (scale bars: 100 $\mu$m).

of the photoresist materials with the aim of realizing a fiber-endoscope objective with a zoom function and promoting the application of micro-optical systems.

## Declaration of competing interest

The authors declare that they have no conflicts of interest in this work.

## Acknowledgments

This work was supported by Shenzhen Science and Technology Program (RCYX20200714114524139, Shenzhen Key Laboratory of Ultrafast Laser Micro/Nano Manufacturing ZDSYS20220606100405013), Natural Science Foundation of Guangdong Province (2022B1515120061), National Natural Science Foundation of China (62122057, 62075136).

## Supplementary materials

Supplementary material associated with this article can be found, in the online version, at doi:10.1016/j.fmre.2022.05.026.

## References


[1] K. Sakitani, T. Nishizawa, M. Arita, et al., Early detection of gastric cancer after Helicobacter pylori eradication due to endoscopic surveillance, Helicobacter. 23 (2018) e12503.

[2] J. Metello, A. Relva, E. Milheras, Hysteroscopic diagnostic accuracy in post–menopausal bleeding, Acta Med. Port. 21 (5) (2008) 483–487.

[3] A. de Faria, C. Dias, L. Moetzsohn, et al., Feasibility of transnasal endoscopy in screening for esophageal and gastric varices in patients with chronic liver disease, Endosc. Int. Open 5 (2017) E646–E651.

[4] A.C. Colvin, N. Egorova, A.K. Harrison, et al., National trends in rotator cuff repair, J. Bone Joint Surg. Am. 94A (2012) 227–233.

[5] K. Suzumori, T. Miyagawa, M. Kimura, et al., Micro inspection robot for 1-in pipes, IEEE/ASME Trans. Mechatronics 4 (3) (1999) 286–292.

[6] S. Martelli, L. Mazzei, C. Canali, et al., Deep endoscope: intelligent duct inspection for the avionic industry, IEEE Trans. Industr. Inform. 14 (4) (2018) 1701–1711.

[7] B. Nelson, I. Kaliakatsos, J. Abbott, Microrobots for minimally invasive medicine, Annu. Rev. Biomed. Eng. 12 (1) (2010) 55–85.

[8] N. Simaan, Snake-like units using flexible backbones and actuation redundancy for enhanced miniaturization, IEEE Int. Conf. Robot. Autom. (2005) 3012–3017.

[9] F. Keus, J.A. de Jong, H.G. Gooszen, et al., Laparoscopic versus open cholecistectomy for patients with symptomatic cholecystolithiasis, Cochrane Library 1 (2009) 1–156.

[10] E. Davis, JW. Roblee, Comparison of freeform manufacturing techniques in the production of monolithic lens arrays, Proc. SPIE 7426 (2009) 742605–742611.

[11] L. Li, A.Y. Yi, Design and fabrication of a freeform microlens array for a compact large-field-of-view compound-eye camera, Appl. Opt. 51 (2012) 1843–1852.

[12] E. Brinksmeier, O. Riemer, Submicron functional surfaces generated by diamond machining, CIRP Ann. Manuf. Technol. 59 (1) (2010) 535–538.

[13] A. Shorey, W. Kordonski, M. Tricard, Deterministic precision finishing of domes and conformal optics, Proc. SPIE 5786 (2005) 310–318.

[14] R. Berg, Extreme UV lithography preserves Moore's Law, Opt. Laser Technol. 129 (2005) 29–31.

[15] B.H. Cumpston, S.P. Ananthavel, S. Barlow, et al., Two-photon polymerization initiators for three-dimensional optical data storage and microfabrication, Nature 398 (1999) 51–54.

[16] H.B. Sun, S. Matsuo, H. Misawa, Three-dimensional photonic crystal structures achieved with two-photon-absorption photopolymerization of resin, Appl. Phys. Lett. 74 (6) (1999) 786–788.

[17] P. Galajda, P. Ormos, et al., Complex micromachines produced and driven by light, Appl. Phys. Lett. 78 (2) (2001) 249–251.

[18] J. Wang, Y. He, H. Xia, et al., Embellishment of microfluidic devices via femtosecond laser micronanofabrication for chip functionalization, Lab. Chip. 10 (5) (2010) 1993–1996.

[19] S. Kawata, H.B. Sun, T. Tanaka, et al., Finer features for functional microdevices, Nature 412 (2001) 697–698.

[20] Y. Cao, Z. Gan, B. Jia, et al., High-photosensitive resin for super-resolution direct-laser-writing based on photoinhibited polymerization, Opt. Express. 19 (2011) 19486–19494.

[21] W. Zhou, An efficient two-photon-generated photoacid applied to positive-tone 3D microfabrication, Science 296 (5570) (2002) 1106–1109.

[22] J. Fischer, M. Wegener, Three-dimensional optical laser lithography beyond the diffraction limit, Laser Photonics Rev. 7 (1) (2013) 22–44.

[23] Z. Gan, Y. Cao, R A Evans, et al., Three-dimensional deep sub-diffraction optical beam lithography with 9 nm feature size, Nat. Commun. 4 (6) (2012) 2061.

[24] Y. Huang, Y.L. Qin, P. Tu, et al., High fill factor microlens array fabrication using direct laser writing and its application in wavefront detection, Opt. Lett. 45 (16) (2020) 4460–4463.

[25] J. Yu, Y.P. Wang, W. Yang, et al., All-fiber focused beam generator integrated on an optical fiber tip, Appl. Phys. Lett. 116 (24) (2020) 241102.

[26] J. Yu, Z. Bai, G. Zhu, et al., 3D nanoprinted kinoform spiral zone plates on fiber facets for high-efficiency focused vortex beam generation, Opt. Express. 28 (25) (2020) 38127–38139.

[27] Z. Xie, S. Gao, T. Lei, et al., Integrated (de)multiplexer for orbital angular momentum fiber communication, Photonics Res. 6 (7) (2018) 743–749.

[28] W. Jia, C. Lin, C. Liao, et al., Bragg resonance in microfiber realized by two-photon polymerization, Opt. Express. 26 (4) (2018) 3732–3737.

[29] L. Chi, C. Liao, J. Wang, et al., Femtosecond laser microprinting of a polymer fiber Bragg grating for high-sensitivity temperature measurements, Opt. Lett. 43 (14) (2018) 3409–3412.

[30] C. Liao, C. Li, C. Wang, et al., High-speed all-optical modulator based on a polymer nanofiber bragg grating printed by femtosecond laser, ACS Appl. Mater. Interfaces 12 (1) (2020) 1465–1473.

[31] P.I. Dietrich, R.J. Harris, M. Blaicher, et al., Printed freeform lens arrays on multi--core fibers for highly efficient coupling in astrophotonic systems, Opt. Express. 25 (15) (2017) 18288–18295.

[32] L. Bremer, K. Weber, S. Fischbach, et al., Quantum dot single-photon emission coupled into single-mode fibers with 3D printed micro-objectives, APL Photonics 5 (10) (2020) 106101.

[33] Z. Li, C. Liao, J. Wang, et al., Femtosecond laser microprinting of a fiber whispering gallery mode resonator for highly-sensitive temperature measurements, J. Lightwave Technol. 31 (4) (2019) 1241–1245.

[34] C. Xiong, J. Zhou, C. Liao, et al., Fiber-tip polymer microcantilever for fast and highly sensitive hydrogen measurement, ACS Appl. Mater. Interfaces 12 (29) (2020) 33163–33172.

[35] M. Zou, C. Liao, S. Liu, et al., Fiber-tip polymer clamped-beam probe for high-sensitivity nanoforce measurements, Light Sci. Appl. 10 (9) (2021) 1768–1779.

[36] P. Ji, M. Zhu, C. Liao, et al., In-fiber polymer microdisk resonator and its sensing applications of temperature and humidity, ACS Appl. Mater. Interfaces. 13 (40) (2021) 48119–48126.

[37] S. Schmidt, S. Thiele, A. Toulouse, et al., Tailored micro-optical freeform holograms for integrated complex beam shaping, Optica 7 (10) (2020) 1279–1286.

[38] T. Gissibl, S. Thiele, A. Herkommer, et al., Sub-micrometre accurate free-form optics by three-dimensional printing on single-mode fibres, Nat. Commun. 7 (2016) 11763.

[39] T. Gissibl, S. Thiele, A. Herkommer, et al., Two-photon direct laser writing of ultracompact multi-lens objectives, Nat. Photonics 10 (8) (2016) 554–560.

[40] P.I. Dietrich, M. Blaicher, I. Reuter, et al., In situ 3D nanoprinting of free-form coupling elements for hybrid photonic integration, Nat. Photonics 12 (4) (2018) 241–247.

[41] S. Thiele, K. Arzenbacher, T. Gissibl, et al., 3D-printed eagle eye: Compound microlens system for foveated imaging, Sci. Adv. 3 (2) (2017) e1602655.

[42] T. Gissibl, S. Wagner, J. Sykora, et al., Refractive index measurements of photo-resists for three-dimensional direct laser writing, Opt. Mater. Express. 7 (7) (2017) 2293–2298.



**Bozhe Li** was born in Hubei, China, in 1997. He received the BEng. degree in the School of Electrical and Electronic Engineering from Chongqing University of Technology, Chongqing, China, in 2019. He is currently pursuing the MEng. degree in the College of Physics and Optoelectronic Engineering from Shenzhen University, Guangdong, China. His research interests include femtosecond laser micro-nano machining technology and optical fiber endoscopic imaging.



**Changrui Liao** (BRID: 08573.00.36759) distinguished professor in College of Physics and Optoelectronic Engineering at Shenzhen University and holds the position of Deputy Director of Guangdong and Hong Kong Joint Research Center for Optical Fiber Sensors and Director of Shenzhen Key Laboratory of Ultrafast Laser Micro and Nano Manufacturing. He received PhD degree from Hong Kong Polytechnic University in 2012 and then joined Shenzhen University and successively served as lecturer, associate professor, and distinguished professor. Prof. Liao's research interests lie in ultrafast laser 3D nanolithography and its application in optical fiber sensors, smart chips, and new energy. He authored/co-authored 2 book chapters, > 190 journal papers, and > 10 patents in 3D nanolithography and optical fiber sensors. His works were cited > 7000 times with an h-index 48 (SCIE).